

www.chemphyschem.org

# A Theoretical Perspective to Study the Optical Properties of Tetrafluoroborates

Jun Sun,\*[a] Zhaofeng Wu,\*[a] Ming-Hsien Lee,[b] and Haiming Duan\*[a]

In this study, a series of tetrafluoroborates with non- $\pi$ -conjugated [BF<sub>4</sub>] tetrahedra are investigated systematically by first-principles calculations. Theoretical studies demonstrate that tetrafluoroborates with alkali and/or alkaline-earth metals are more favorable for deep-ultraviolet transmission and are comparable to the classical deep-ultraviolet (deep-UV) material, MgF<sub>2</sub>. Furthermore, bandgap decrease with the increasing of ionic radii in alkali and/or alkaline-earth metals. Introducing highly polarizable cations with  $d_{10}$ -configuration or cations with lone pair electrons into the structure will decrease the

bandgaps. The birefringence and second harmonic generation effects are not large enough in tetrafluoroborates because polarizability anisotropy and hyperpolarizability in  $non-\pi$ -conjugated [BF<sub>4</sub>] tetrahedra are much smaller than those in  $\pi$ -conjugated groups. However, the second harmonic generation effect for [BF<sub>4</sub>] tetrahedra has a higher contribution in comparison with that due to birefringence. To effectively synthesize the borate fluorides or fluorooxoborates in the deep-UV region, raw materials with B–F bonds are preferred.

#### Introduction

Deep-ultraviolet (deep-UV,  $\lambda$  < 200 nm,  $E_g$  > 6.2 eV) materials play an important role in optical communication and the laser industry, such as nonlinear optical (NLO), birefringent, and self-frequency-doubling laser materials. [1-14] Borates have been great contenders in the search for new UV optical materials in recent years due to their flexible structures. [1,5,15-19] Metal borates have wider transmission ranges in the UV region owing to the substantial difference in the electronegativity of boron and oxygen atoms. [20,21] Over the past few decades, a series of borate-based compounds have been developed, including  $\alpha$  and  $\beta$ -BaB<sub>2</sub>O<sub>4</sub>, [22,23] LiB<sub>3</sub>O<sub>5</sub>, [24] CsB<sub>3</sub>O<sub>5</sub>, [25] and well-known deep-UV material KBe<sub>2</sub>BO<sub>3</sub>F<sub>2</sub> (KBBF), [26] and many other reported borate crystals such as Gd<sub>4</sub>B<sub>4</sub>O<sub>11</sub>F<sub>2</sub>, [27] Ba<sub>2</sub>M(B<sub>3</sub>O<sub>6</sub>)<sub>2</sub> (M = Mg and Ca), [28-29] Sr<sub>2</sub>Be<sub>2</sub>B<sub>2</sub>O<sub>7</sub>, [30] K<sub>5</sub>Ba<sub>2</sub>(B<sub>10</sub>O<sub>17</sub>)<sub>2</sub>(BO<sub>2</sub>), [31] and Ca(BO<sub>2</sub>)<sub>2</sub>. [32]

Theoretical and experimental studies have shown that the addition of fluorine into borates results in borate fluorides or fluorooxoborates, [21,27,33-38] which not only expands the structural diversity but also improves the optical properties such as bandgaps, birefringence, and second harmonic generation (SHG). [5,20-21,39-41] For bandgaps, the fluorine with the largest electronegativity can eliminate the dangling bonds of terminal oxygen, and blue shifts the absorption edges. Also, fluorine can

substitute for oxygen to form oxyfluoride  $[BO_{4x}F_x]$  (x=1, 2, 3, abbreviated as [BOF]) units with strong polarizability anisotropy and hyper-polarizability, which are beneficial for a larger bandgap and wider deep-UV transmittance. The [BOF] units will become [BF<sub>4</sub>] units by replacing all the four O atoms with F atoms, resulting in tetrafluoroborates, such as BaCl(BF4) (180 nm).[42] There are more studies on fluorooxoborates compared to tetrafluoroborates. However, tetrafluoroborates were often chosen as raw materials in the synthesis of new compounds. So, tetrafluoroborates have come into the scope of our research along with questions regarding UV cutoff edges, birefringence, structures, or SHG coefficients. Currently, there are few theoretical studies on tetrafluoroborates. The available anhydrous tetrafluoroborate (composition search criteria: B. F-O; "-" means exclude the related elements) were checked by screening the web-assisted inorganic crystal structure database (ICSD with version 4.2.0, the latest release of ICSD-2020/ 09/04)[43] and have been investigated theoretically and summarized in this paper.

#### **Results and Discussion**

#### **Space Group Statistics and Crystal Structure**

In the current study, all the tetrafluoroborates with reasonable structures were considered as the source data to investigate the structure-properties relationship (Table S3, SI). The bond lengths of B—F and space group statistics are summarized as follows:

(1) The bond lengths of B cations and F anions range from 1.242 to 1.529 Å, which agree with reasonable values. As shown in Figure 1, most of the B–F bond lengths are distributed in the range of 1.341–1.440 Å (82.04%). The shortest bond length (1.240-1.290 Å, 0.78%) exists in only one case,  $Sn_5F_9(BF_4)$ , whereas the longest bond length (1.491–1.540 Å, 5.47%) is only found in one compound,  $Ba_2(BF_4)$ ,  $I_4^{[45]}$ 

 J. Sun, Z. Wu, Prof. H. Duan School of Physical Science and Technology Xinjiang University 777 Huarui Road, Urumqi 830017, China E-mail: sunjun@xju.edu.cn wuzf@xju.edu.cn dhm@xju.edu.cn

[b] Prof. M.-H. Lee Department of Physics, Tamkang University New Taipei City 25137, Taiwan

Supporting information for this article is available on the WWW under https://doi.org/10.1002/cphc.202200205

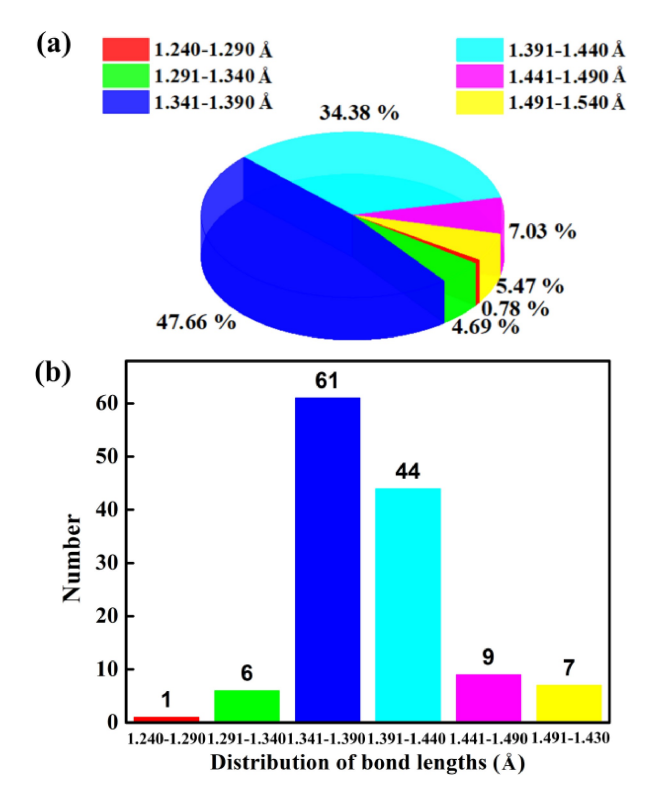


Figure 1. The bond lengths of B-F in tetrafluoroborates.

(2) The obtained statistics from Figure 2 and Table S3 show that the tetrafluoroborates span the five crystal systems: monoclinic, orthorhombic, tetragonal, trigonal, and hexagonal systems. The related proportions are found to be 30.77, 53.85, 3.85, 3.85, and 7.69% for these five branches, respectively. Among them, the most common space group is orthorhombic Pnma (No. 62), and nearly 30.77% of the tetrafluoroborates are crystallized in this space group. In addition, P2<sub>1</sub>/c (No. 14) and Pbca (No. 61) make up the rest of the top three types of space groups. For the remaining types, there are eight space groups, including C2/m, Pmn2<sub>1</sub>, Imm2, Cmcm, I4<sub>1</sub>/amd, P3<sub>1</sub>21, P2 m, P6<sub>3</sub>/ mmc. Only seven crystallographic point groups are found: 2/m, mm2, mmm, 4/mmm, 32, m and 6/mmm, respectively. Most tetrafluoroborates crystallize in the centrosymmetric (CS) space group except for  $BaCI(BF_4)$ , [42]  $K_3Na_4(SiF_6)_3(BF_4)$ , [46]  $Ba(BF_4)(PF_6)$ , [47] and Li(BF<sub>4</sub>)<sup>[48]</sup> which are crystallized in the non-centrosymmetric (NCS) space group. Apart from  $Li_2F(BF_4)$ , [49]  $Ba(BF_4)(PF_6)$ , [47]  $Ba_2(BF_4)_2(AsF_6)(H_3F_4)$ , [47] and  $Li(BF_4)$ , [48] which belongs to biaxial crystals, the vast majority of tetrafluoroborates are uniaxial crystals.

Alkali or alkali earth metal-tetrafluoroborates that are free of d-d or f-f electronic transitions are considered first. The B atoms are tetrahedrally coordinated with the F atoms, forming the [BF $_4$ ] tetrahedra. For the IA group, they all crystallize in the monoclinic system, whereas Li(BF $_4$ )[48] crystallizes in the trigonal system with higher symmetry. Figure S1 in the SI shows their structures. For Li(BF $_4$ ),[48] there is one Li, one B, and two F atoms in an asymmetric unit. Li atoms are tetra-coordinated to F atoms to form [LiF $_4$ ] tetrahedra, and this form two-dimensional

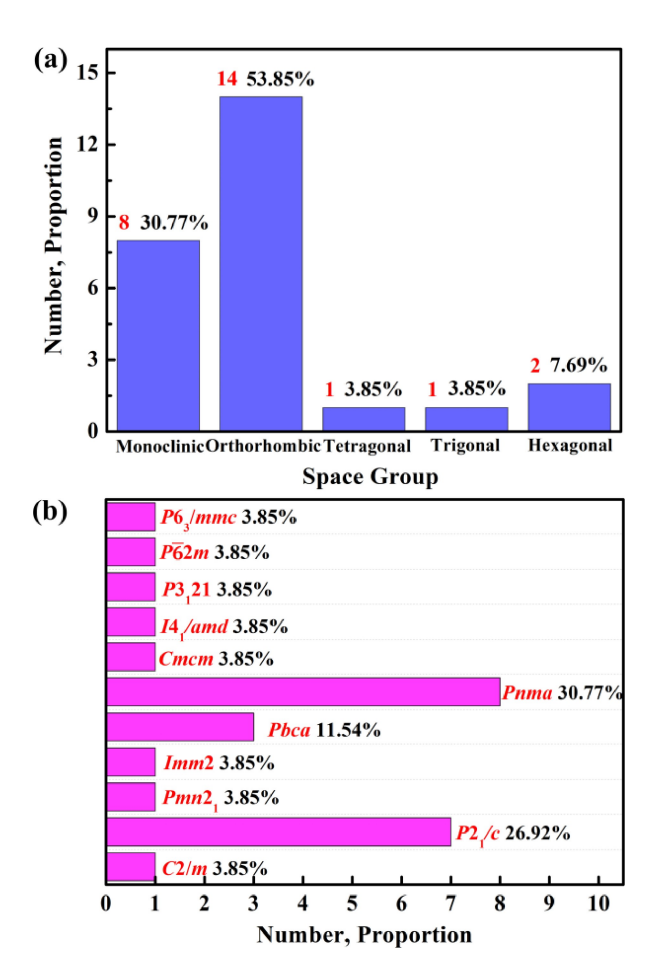


Figure 2. Analysis of space group and crystallographic point groups of tetrafluoroborates.

(2D) layers with [BF<sub>4</sub>] tetrahedra. These 2D layers are further connected by the F atoms to form the final three-dimensional (3D) network (Figure S1a, SI). For Na(BF<sub>4</sub>), [50] there is one unique Na, one unique B, and two unique F atoms in its asymmetric unit. Na atoms are bonded to eight F atoms to form [NaF<sub>8</sub>] polyhedra, which combine to [BF<sub>4</sub>] tetrahedra to form the 3D network (Figure S1b, SI). For A(BF<sub>4</sub>) (A = K, Rb, Cs),  $^{[51,52]}$  there is one unique K/Rb/Cs, one B, and three F atoms in their asymmetric units, respectively. K atoms are linked to ten F atoms to form [KF<sub>10</sub>] polyhedra. Rb/Cs atoms are linked to twelve F atoms to form [Rb/CsF<sub>12</sub>] polyhedra. They form a 3D framework by combining with the [BF<sub>4</sub>] tetrahedra (Figures S1c, S1d and S1e, SI). For the IIA group,  $Ca(BF_4)_2^{[53]}$  and  $Sr(BF_4)_2^{[45,54]}$ crystallize in the monoclinic system with similar structures whereas  $Ba(BF_4)_2^{[45]}$  and  $Ba_2(BF_4)_4^{[55]}$  crystallize in the orthorhombic system. Their structures are shown in Figure S2 in the SI. For  $M(BF_4)_2$  (M=Ca, Sr), [45,53,54] the asymmetric unit contains one, two, and eight crystallographic-independent M, B, and F atoms, respectively. M atoms are octa-coordinated to F atoms, forming [MF<sub>8</sub>] polyhedra. [MF<sub>8</sub>] polyhedra and [BF<sub>4</sub>] tetrahedra make up the final 3D network by sharing F atoms (Figures S2a and S2b, SI). Ba(BF<sub>4</sub>)<sub>2</sub><sup>[45]</sup> has one Ba, one B, and three F atoms in an asymmetric unit. Ba atoms are coordinated with ten F atoms to



form  $[BaF_{10}]$  polyhedra that further link together to form one-dimensional (1D) chains by edge-sharing (Figure S3a, SI). The 1D chains are composed of a 3D network by  $[BF_4]$  tetrahedra (Figures S2c, SI).  $Ba_2(BF_4)_4$ ,  $^{[45]}$  have two Ba, four B, and sixteen F atoms. Ba atoms are nine-coordinated to F atoms, forming  $[BaF_9]$  polyhedra. As shown in Figure S3b in SI, two  $[BaF_9]$  polyhedra are formed to an isolated  $[Ba_2F_{16}]$  unit by edge-sharing. The isolated  $[Ba_2F_{16}]$  units make up a 3D network by  $[BF_4]$  tetrahedra (Figures S2d, SI).

#### **Electronic Structure**

Figure 3 shows the plotted values of the bandgaps for the tetrafluoroborates using the HSE06 method. Some tetrafluoroborates, including A(BF4) (A = NH4, Li, Na, K, Rb, Cs),  $^{[48,50-52]}$  $M(BF_4)_2$  (M = Ca, Sr, Ba), [45,53,54] and Ba(BF<sub>4</sub>)(PF<sub>6</sub>)[47] have advantages in deep-UV transmission when compared to the famous deep-UV material, MgF<sub>2</sub> (130 nm, corresponding to 9.538 eV). [56] Alkali and/or alkaline earth-metal tetrafluoroborates have been suggested as potential materials for the deep-UV transmission range (Table S4, SI). The deep-UV cutoff edge of BaCl(BF<sub>d</sub>)<sup>[42]</sup> is about 180 nm, corresponding to 6.889 eV. As a consequence of the difference of exchange-correlation, its calculated bandgap is 5.55 eV which is smaller than that reported in this paper. Figures S4 and S5 in the SI show the partial density of states (PDOS), which are calculated by GGA-PBE of A(BF<sub>4</sub>) (A = Li, Na, K, Rb, Cs)<sup>[48,50–52]</sup> and M(BF<sub>4</sub>)<sub>2</sub> (M=Ca, Sr, Ba), [45,53,54]</sub> respectively. In the  $A(BF_a)^{[48,50-52]}$  and  $M(BF_a)_2^{[45,53,54]}$  tetrafluoroborates series, near the top of the valence bands (VBs) is mainly occupied by F 2p orbitals while the bottom edges of the conduction bands (CBs) are mainly dominated by A/M s orbitals (Figures S4 and S5 in the SI). This indicates that the bandgaps of the two series of tetrafluoroborates are controlled by A/M-F units. As the F 2p orbitals in the two series of tetrafluoroborates are mostly occupied near the top of the VBs, only the bottom of the CBs is of concern now. In Figure 4, the F 2p orbitals and A/M s orbitals are plotted. The distance between the Cs s orbitals and the

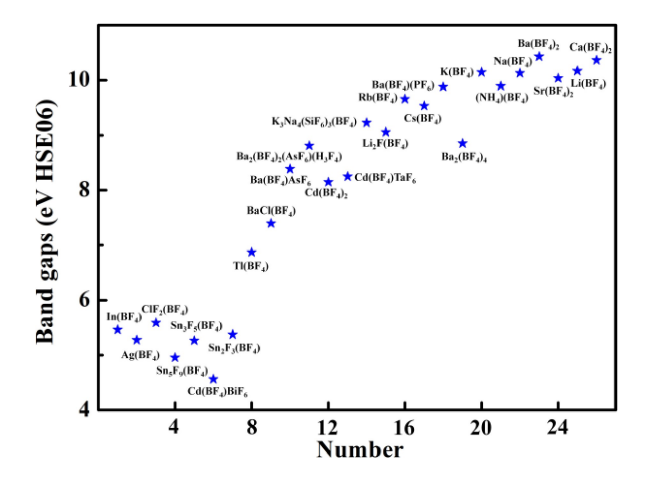


**Figure 3.** The values of bandgaps for tetrafluoroborates under the condition of HSE06.

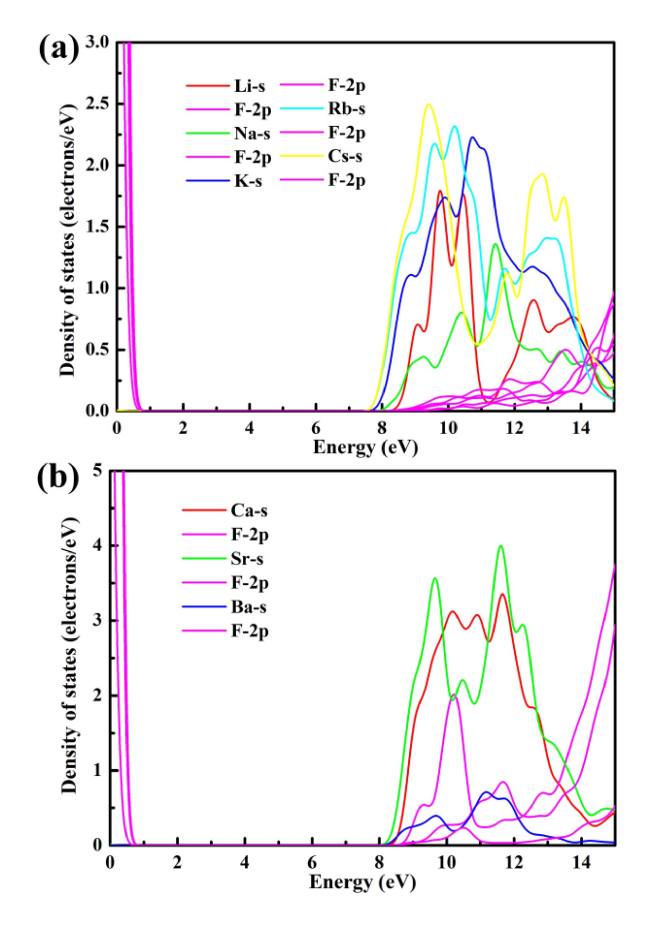


**Figure 4.** The A/M s orbitals and F 2p orbitals in the series of (a) A(BF<sub>4</sub>) and (b) M(BF<sub>4</sub>)<sub>2</sub> tetrafluoroborates.

Fermi surface is shorter than that between the Li s orbitals and the Fermi surface, resulting in the values of bandgaps for  $Cs(BF_4)^{[51]}$  being smaller than that for  $Li(BF_4)^{[48]}$  (Figure 4a). The differences in distances between M s orbitals and the Fermi surface are very small, which leads to slight differences in their bandgaps. However, their bandgaps still follow this rule:  $Ca(BF_4)_2^{[53]} > Sr(BF_4)_2^{[45,54]} > Ba(BF_4)_2^{[45]}$  (Figure 4b). Thus, as the cation radius increases, the closer the A/M s orbitals are to the Fermi surface, the smaller the bandgaps (Figures 4, S4 and S5).

When cations with a lone pair or highly polarizable cations are introduced into tetrafluoroborates, the cutoff edge is redshifted. This corresponds to the smaller bandgaps like Cd- $(BF_4)_2^{[45,57]}$  with 6.580 eV,  $Sn_5F_9(BF_4)^{[44]}$  with 3.597 eV. Figure S6 in SI describes the PDOS of  $Li(BF_4)$ , [48]  $Ca(BF_4)$ , [53]  $Cd(BF_4)$ , [45,57] and Sn<sub>s</sub>F<sub>o</sub>(BF<sub>d</sub>)<sup>[44]</sup> calculated by GGA-PBE. Near the top of VBs and the bottom of CBs are mainly occupied by F 2p orbitals and Li/ Ca/Cd s orbitals, respectively (Figures S6a, S6b, and S6c, SI), except for  $Sn_5F_0(BF_4)$ , which is occupied by Sn 5 s, Sn 5p, F 2p, and Sn 5p orbitals, respectively (Figure S6d, SI). This phenomenon indicates that the materials containing the lone pair or highly polarizable cations are unsuitable as potential deep-UV transmission materials. The PDOS of Sn<sub>s</sub>F<sub>o</sub>(BF<sub>d</sub>)<sup>[44]</sup> is different from other tetrafluoroborates such as A(BF<sub>4</sub>), [48,50-52] M- $(BF_4)_2^{[45,53,54]}$  and  $Cd(BF_4)_2^{[45,57]}$  In Figure S7 in SI, the PDOS of other Sn-containing tetrafluoroborates such as Sn<sub>3</sub>F<sub>5</sub>(BF<sub>4</sub>) and



Sn<sub>2</sub>F<sub>3</sub>(BF<sub>4</sub>)<sup>[58]</sup> are plotted. As depicted in Figure S7 in SI, near the bottom of the CBs for  $Sn_3F_5(BF_4)$  and  $Sn_2F_3(BF_4)^{[58]}$  are the same as Sn<sub>5</sub>F<sub>9</sub>(BF<sub>4</sub>), [44] which are predominantly dominated by Sn 5p orbitals. As shown in Figure S7a in SI, there are Sn 5 s, Sn 5p, and F 2p orbitals near the top of the VBs for  $Sn_3F_5(BF_4)^{[58]}$  similar to  $Sn_5F_9(BF_4)$ , [44] while for  $Sn_2F_3(BF_4)$ , [58] there are  $Sn\ 5\ s$  and Sn5p orbitals (Figure S7b, SI). To analyze the differences near the top of the VBs in the three Sn-containing tetrafluoroborates, the coordination environments of cations have been considered. The coordination environment of B atoms is bonded to the four F atoms to form [BF<sub>4</sub>] tetrahedra, while that of Sn atoms is different (Figure S8, SI). In  $Sn_5F_9(BF_4)^{[44]}$  and  $Sn_3F_5(BF_4)^{[58]}$  the Snatoms are not only bonded to three F atoms to form [SnF<sub>3</sub>] units but also bonded to four F atoms to form [SnF<sub>4</sub>] groups (Figures S8a and S8b, SI). But in Sn<sub>2</sub>F<sub>3</sub>(BF<sub>4</sub>), [44] there is one coordination environment of Sn atoms coordinating to three F atoms to construct [SnF<sub>3</sub>] units (Figure S8c, SI). This may explain the differences near the top of VBs for the three Sn-containing tetrafluoroborates.

#### **Optical Properties**

Birefringence is a very important property of optical crystal materials. The calculated values are given in Table S2 in SI. The calculations show that tetrafluoroborates have very small birefringence because there are no  $\pi$ -conjugated groups in those structures. However, five tetrafluoroborates have larger In(BF<sub>4</sub>)<sup>[59]</sup> birefringence than others. which include  $0.047@1064 \text{ nm}, \quad CIF_{2}(BF_{4})^{[60]} \quad 0.193@1064 \text{ nm}, \quad Sn_{5}F_{9}(BF_{4})^{[44]}$ 0.047@1064 nm,  $Sn_3F_5(BF_4)^{[58]}$  0.073@1064 nm,  $Sn_2F_3(BF_4)^{[44]}$ 0.052@1064 nm. The real space atom cutting (RSAC)  $^{\rm [61]}$  method was used to analyze the birefringence contribution of the [BF<sub>4</sub>] tetrahedral group quantitatively. During RSAC operation, the cutting radii follow the basic principle of "keeping the atomic spheres in contact with each other without overlapping". The cutting radii of B and F atoms for the five compounds are set to 0.20 Å (B), 1.20 Å (F), respectively. The cutting radii of other atoms are set as follows: for  $In(BF_4)$ , [58] 0.74 Å (In); for  $CIF_2(BF_4)$ , [60] 0.42 Å (CI); for  $Sn_5F_9(BF_4)$ , [44] 0.76 Å (Sn); for  $Sn_3F_5(BF_4)$ , [57] 0.87 Å (Sn); for  $Sn_2F_3(BF_4)$ , [57] 0.73 Å (Sn). The [BF<sub>4</sub>] tetrahedral groups are cut, and the obtained contributions are shown in Table 1. Regarding the five tetrafluoroborates, the non- $\pi$ -conjugated [BF<sub>4</sub>] tetrahedral groups make little contribution to the birefringence except for  $CIF_2(BF_4)$ . [60] In short, the non- $\pi$ conjugated [BF<sub>4</sub>] tetrahedron is not a "good gene" to synthesize birefringent materials.

Table 1. The calculated birefringence and the RSAC analysis.		
Birefringence (@1064 nm) compounds	Original	After RSAC
In(BF <sub>4</sub> ) CIF <sub>2</sub> (BF <sub>4</sub> ) Sn <sub>2</sub> F <sub>3</sub> (BF <sub>4</sub> ) Sn <sub>3</sub> F <sub>5</sub> (BF <sub>4</sub> ) Sn <sub>5</sub> F <sub>9</sub> (BF <sub>4</sub> )	0.047 0.193 0.052 0.073 0.047	0.040 0.122 0.051 0.083 0.051

There are four tetrafluoroborates crystallized in non-centrosymmetric space groups. Their SHG coefficients are also calculated  $(d_{ii} < 0.010 \text{ pm/V})$  is omitted), including BaCl(BF<sub>4</sub>),  $d_{15} = 0.103 \text{ pm/V}, \quad d_{33} = -0.265 \text{ pm/V}; \quad K_3 Na_4 (SiF_6)_3 (BF_4), \quad d_{24} = 0.103 \text{ pm/V}$ 0.057 pm/V; Ba(BF<sub>4</sub>)(PF<sub>6</sub>),  $d_{16} = -0.017$  pm/V,  $d_{22} = 0.017$  pm/V; Li(BF<sub>4</sub>),  $d_{16} = -0.087$  pm/V,  $d_{22} = 0.087$  pm/V. The birefringence of these tetrafluoroborates is 0.001@1064 nm except for BaCl(BF<sub>4</sub>) whose birefringence is 0.014@1064 nm. Hence, BaCl(BF<sub>4</sub>) is of interest. According to the results from Figure 5, we found that the main contributions of the occupied and unoccupied states are the F atoms, B atoms, and Cl atoms with a little contribution, respectively, which indicates the [BF<sub>4</sub>] tetrahedral groups dominant the SHG response. According to the anionic group theory, as the cation contribution for SHG is very small, the total SHG response is also very weak. [62] The [BF<sub>4</sub>] tetrahedral groups are cut by using the RSAC method. Consequently, the SHG coefficients decrease  $(d_{15} = 0.995 \times$  $10^{-4}$  pm/V,  $d_{33} = 0.677 \times 10^{-2}$  pm/V). Thus, the non- $\pi$ -conjugated tetrahedral groups play a significant role in the SHG response for NLO materials that do not contain the planar units.

# **Conclusions**

To summarize, the first-principles method was used to investigate the electronic structures and related optical properties of tetrafluoroborates with non- $\pi$ -conjugated [BF<sub>4</sub>] tetrahedra. The theoretical studies reveal that tetrafluoroborates are beneficial

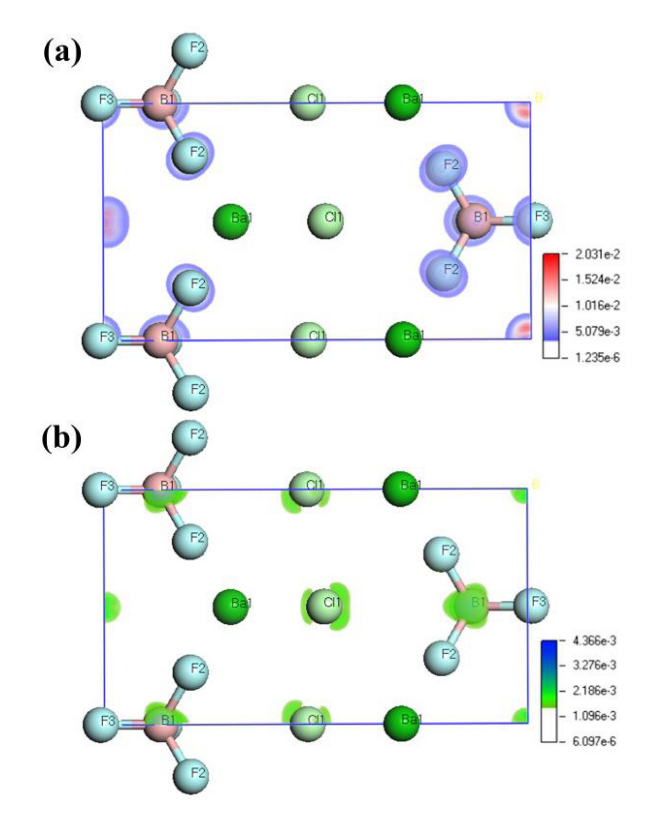


Figure 5. The SHG density of (a) occupied and (b) unoccupied in BaCl(BF<sub>4</sub>).



to have deep-UV region transmission that are comparable to classical deep-UV materials such as MgF<sub>2</sub>. Moreover, the bandgaps decrease with the increasing of cation radii for alkali or alkaline earth metals. When the cations with lone pair electrons or highly polarizable cations with  $d^{10}$ -configuration are introduced into the structures, the bandgaps decrease due to the different distances between s/p orbitals and the Fermi surface. Also, the birefringence and SHG effects are not very large in tetrafluoroborates because of the little polarizability anisotropy and hyperpolarizability in non- $\pi$ -conjugated [BF<sub>4</sub>] tetrahedra. Therefore, the contribution of [BF<sub>4</sub>] tetrahedra to the birefringence is small. However, [BF<sub>4</sub>] tetrahedra play an important role in the SHG response for the compounds which do not contain planar units by using the RSAC method.

# **Computational Section**

The plane wave pseudo-potential method based on the density functional theory (DFT) in the CASTEP package<sup>[63,64]</sup> was used to calculate the electronic structures and optical properties of tetrafluoroborates. During the calculation, the exchange-correlation potential was based on the generalized gradient approximation (GGA) with the Perdew-Burke-Ernzerhof (PBE) functional. [65] The norm-conserving pseudopotentials (NCP)[66,67] in the Kleinman-Bylander form were used to treat valence electrons: Li 2s1, Na  $2s^22p^63s^1$ . K  $3s^23p^64s^1$ , Rb  $4s^24p^65s^1$ , Cs  $5s^25p^66s^1$ , Ca  $3s^23p^64s^2$ , Sr  $4s^24p^65s^2$ , Ba  $5s^25p^66s^2$ , Sn  $5s^25p^2$ , In  $5s^25p^1$ , As  $4s^24p^3$ , Ta  $5d^36s^2$ , Cd  $4d^{10}5s^2$ , Bi  $5d^{10}6s^26p^3$ , Ag  $4s^24p^64d^{10}5s^1$ , TI  $5d^{10}6s^26p^1$ , B  $2s^22p^1$ , F  $2s^22p^5$ , CI  $3s^23p^5$ , N  $2s^22p^3$ , P  $3s^23p^3$ . In this paper, the non-local exchange functional HSE06<sup>[68,69]</sup> was used to obtain more accurate values of bandgaps. HSE06 is a widely used hybrid functional with relatively high efficiency and can evaluate the optical bandgap of the material in the absence of the experimental bandgap. And, in order to ensure the consistency between the experimental and the calculated results, the scissors operator was adopted in this manuscript, where the scissors operator was set as the difference between the HSE06 functional and GGA-PBE band gaps. [33,39,70] The kinetic energy cutoff for all the compounds in the simulation of tetrafluoroborates is 940 eV. Table S1 in the SI lists the Monkhorst-Pack k-points of tetrafluoroborates.

The imaginary part of the dielectric function  $\varepsilon_2$ , which is based on electronic structures, can be calculated, and its real part is determined by the Kramers-Kronig transformation. Then, the refractive indices and the birefringence  $\Delta n$  can be obtained. The difference between the GGA-PBE and HSE06, which are listed in Table S2 in the SI, was used to scissor-correct the optical properties calculation. [33,39,70] The SHG coefficients were calculated by the CASTEP package using the calculated band structures (Table S2, SI). At the limit of zero frequency, the second-order nonlinear susceptibilities,  $\chi_{\alpha\beta\gamma}^{(2)}(0)$ , can be expressed as the sum of the contribution of the virtual-electron (VE) processes and the virtual-hole (VH) processes:

$$\chi^{(2)}_{\alpha\beta\gamma} = \chi^{(2)}_{\alpha\beta\gamma}(\mathrm{VE}) + \chi^{(2)}_{\alpha\beta\gamma}(\mathrm{VH})$$

$$\chi^{(2)}_{\alpha\beta\gamma}(\mathrm{VE}) = \frac{e^3}{2\hbar m^3} \sum_{vcc'} \int \frac{d^3k}{4\pi^3} P(\alpha\beta\gamma) Im \left[ P^\alpha_{cv} P^\beta_{cc'} P^\gamma_{c'v} \right] (\frac{1}{\omega^3_{cv} \omega^2_{vc'}} + \frac{2}{\omega^4_{vc} \omega_{c'v}})$$

$$\chi^{(2)}_{\alpha\beta\gamma}(\mathrm{VH}) = \frac{e^3}{2\hbar m^3} \sum_{vv'c} \int \frac{d^3k}{4\pi^3} P(\alpha\beta\gamma) \, Im \left[ P^\alpha_{vv'} P^\beta_{cv'} P^\gamma_{cv} \right] (\frac{1}{\omega^3_{cv} \omega^2_{v'c}} + \frac{2}{\omega^4_{vc} \omega_{cv'}}) \, . \label{eq:chi}$$

Here,  $\alpha$ ,  $\beta$ ,  $\gamma$  subscripts show Cartesian components while v, v', and c, c' denote the valence bands (VBs) and conduction bands (CBs).  $P(\alpha\beta\gamma)$ ,  $\omega_{ij}$  and  $P_{ij}{}^{\alpha}$  denote full permutation, band energy difference, and momentum matrix elements, respectively.<sup>[71]</sup>

# **Acknowledgements**

This work was financially supported by the National Natural Science Foundation of China (Grant NOs. 21964016, 11664038), Tianshan Innovation Team Program of Xinjiang Uygur Autonomous Region (Grand NO. 2020D14038), and Tianchi Talent Program (Grand NO. TCBS202131).

### **Conflict of Interest**

The authors declare no conflict of interest.

# **Data Availability Statement**

The data that support the findings of this study are available from the corresponding author upon reasonable request.

**Keywords:** non- $\pi$ -conjugated tetrahedra · deep-ultraviolet optical materials · first-principles calculations · data statistics · optical properties

- [1] M. Mutailipu, K. R. Poeppelmeier, S. L. Pan, Chem. Rev. 2021, 121, 1130– 1202.
- [2] J. Chen, C. L. Hu, F. Kong, J. G. Mao, Acc. Chem. Res. 2021, 54, 2775– 2783.
- [3] P. Becker, Adv. Mater. 1998, 10, 979–992.
- [4] S. Trofimenko, Chem. Rev. 1993, 93, 943–980.
- [5] Y. G. Shen, S. G. Zhao, J. H. Luo, Coord. Chem. Rev. 2018, 366, 1–28.
- [6] G. Aka, A. Brenier, Opt. Mater. 2003, 22, 89-94.
- [7] A. Brenier, J. Lumin. 2000, 91, 121-132.
- [8] F. L. Qin, R. K. Li, J. Cryst. Growth 2011, 318, 642-644.
- [9] C. T. Chen, T. Sasaki, R. K. Li, Y. C. Wu, Z. S. Lin, Y. Mori, Z. G. Hu, J. Y. Wang, S. Uda, M. Yoshimura, *Nonlinear Optical Borate Crystals: Principles and Application*, Wiley-VCH: Weinheim, Germany, 2012.
- [10] H. W. Yu, M. L. Nisbet, K. R. Poeppelmeier, J. Am. Chem. Soc. 2018, 140, 8868–8876.
- [11] H. W. Huang, J. Y. Yao, Z. S. Lin, X. Y. Wang, R. He, W. J. Yao, N. X. Zhai, C. T. Chen, Angew. Chem. Int. Ed. 2011, 50, 9141–9144; Angew. Chem. 2011, 123, 9307–9310.
- [12] T. Sasaki, Y. Mori, M. Yoshimura, Y. K. Yap, T. Kamimura, *Mater. Sci. Eng. R.* 2000, 30, 1–54.
- [13] T. Kiss, F. Kanetaka, T. Yokoya, T. Shimojima, K. Kanai, S. Shin, Y. Onuki, T. Togashi, C. Zhang, C. T. Chen, S. Watanabe, *Phys. Rev. Lett.* 2005, 94, 057001.
- [14] T. Kanai, X. Y. Wang, S. Adachi, S. Watanabe, C. T. Chen, Opt. Express 2009, 17, 8696–8703.
- [15] T. T. Tran, H. Yu, J. M. Rondinelli, K. R. Poeppelmeier, P. S. Halasyamani, Chem. Mater. 2016, 28, 5238–5258.
- [16] W. J. Yao, R. He, X. Y. Wang, Z. S. Lin, C. T. Chen, Adv. Opt. Mater. 2014, 2, 411–417.
- [17] E. L. Belokoneva, Crystallogr. Rev. 2005, 11, 151-198.
- [18] R. Bubnova, S. Volkov, B. Albert, S. Filatov, Crystals 2017, 7, 93.
- [19] M. Mutailipu, S. L. Pan, Angew. Chem. Int. Ed. 2020, 59, 20302–20317; Angew. Chem. 2020, 132, 20480–20496.
- [20] M. Mutailipu, M. Zhang, Z. H. Yang, S. L. Pan, Acc. Chem. Res. 2019, 52, 791–801.



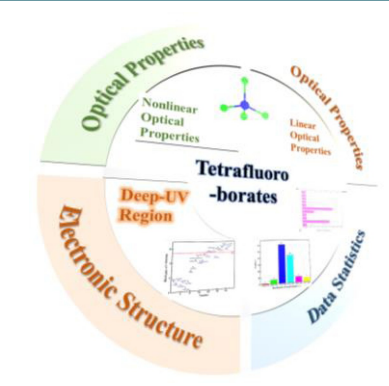
- [21] M. Mutailipu, M. Zhang, B. B. Zhang, L. Y. Wang, Z. H. Yang, X. Zhou, S. L. Pan, Angew. Chem. Int. Ed. 2018, 57, 6095–6099; Angew. Chem. 2018, 130, 6203–6207.
- [22] G. Q. Zhou, J. Xu, X. D. Chen, H. Y. Zhong, S. T. Wang, K. Xu, P. Z. Deng, F. X. Gan, J. Cryst. Growth 1998, 191, 517–519.
- [23] C. T. Chen, B. C. Wu, A. D. Jiang, G. M. You, Sci. China Ser. B 1985, 28, 235–243.
- [24] C. T. Chen, Y. C. Wu, A. D. Jiang, B. C. Wu, G. M. You, R. K. Li, S. J. Lin, *J. Opt. Soc. Am. B* **1989**, *6*, 616–621.
- [25] Y. C. Wu, T. Sasaki, S. Nakai, A. Yokotani, H. G. Tang, C. T. Chen, Appl. Phys. Lett. 1993, 62, 2614–2615.
- *Phys. Lett.* **1993**, 62, 2614–2615. [26] C. T. Chen, G. L. Wang, X. Y. Wang, Z. Y. Xu, *Appl. Phys. B* **2009**, *97*, 9–25.
- [27] A. Haberer, R. Kaindl, H. Huppertz, *J. Solid State Chem.* **2010**, *183*, 471–
- [28] Z. Jia, N. N. Zhang, Y. Y. Ma, L. W. Zhao, M. J. Xia, R. K. Li, Cryst. Growth Des. 2017, 17, 558–562.
- [29] R. K. Li, Y. Y. Ma, CrystEngComm 2012, 14, 5421-5424.
- [30] C. T. Chen, Y. B. Wang, B. C. Wu, K. C. Wu, W. L. Zeng, L. H. Yu, Nature 1995, 373, 322–324.
- [31] C. M. Huang, M. Mutailipu, F. F. Zhang, K. J. Griffith, C. Hu, Z. H. Yang, J. M. Griffin, K. R. Poeppelmeier, S. L. Pan, Nat. Commun. 2021, 12, 2597.
- [32] X. L. Chen, B. B. Zhang, F. F. Zhang, Y. Wang, M. Zhang, Z. H. Yang, K. R. Poeppelmeier, S. L. Pan, J. Am. Chem. Soc. 2018, 140, 16311–16319.
- [33] G. Q. Shi, Y. Wang, F. F. Zhang, B. B. Zhang, Z. H. Yang, X. L. Hou, S. L. Pan, K. R. Poeppelmeier, J. Am. Chem. Soc. 2017, 139, 10645–10648.
- [34] X. F. Wang, Y. Wang, B. B. Zhang, F. F. Zhang, Z. H. Yang, S. L. Pan, Angew. Chem. Int. Ed. 2017, 56, 14119–14123; Angew. Chem. 2017, 129, 14307–14311.
- [35] M. Luo, F. Liang, Y. X. Song, D. Zhao, F. Xu, N. Ye, Z. S. Lin, J. Am. Chem. Soc. 2018, 140, 3884–3887.
- [36] Y. Wang, B. B. Zhang, Z. H. Yang, S. L. Pan, Angew. Chem. Int. Ed. 2018, 57, 2150–2154; Angew. Chem. 2018, 130, 2172–2176.
- [37] C. C. Jin, X. P. Shi, H. Zeng, S. J. Han, Z. Chen, Z. H. Yang, M. Mutailipu, S. L. Pan, Angew. Chem. Int. Ed. 2021, 60, 20469–20475.
- [38] S. G. Jantz, M. Dialer, L. Bayarjargal, B. Winkler, L. van Wüllen, F. Pielnhofer, J. Brgoch, R. Weihrich, H. A. Höppe, Adv. Opt. Mater. 2018, 6, 1800497
- [39] B. B. Zhang, G. Q. Shi, Z. H. Yang, F. F. Zhang, S. L. Pan, Angew. Chem. Int. Ed. 2017, 56, 3916–3919; Angew. Chem. 2017, 129, 3974–3977.
- [40] M. Xia, F. M. Li, M. Mutailipu, S. J. Han, Z. H. Yang, S. L. Pan, Angew. Chem. Int. Ed. 2021, 60, 14650–14656.
- [41] C. C. Jin, H. Zeng, F. F. Zhang, H. T. Qiu, Z. H. Yang, M. Mutailipu, S. L. Pan, Chem. Mater. 2022, 34, 440–450.
- [42] M. Zhang, S. L. Pan, Z. H. Yang, Y. Wang, X. Su, Y. Yang, Z. J. Huang, S. J. Han, K. R. Poeppelmeier, J. Mater. Chem. C 2013, 1, 4740–4745.
- [43] Inorganic Crystal Structure Database. National Institute of Standards and Technology, 2020.
- [44] J. Bonisch, G. Bergerhoff, Acta Crystallogr. Sect. C 1984, 40, 2005–2006.

- [45] T. Bunic, G. Tavcar, E. Goreshnik, B. Zemva, Acta Crystallogr. Sect. C 2007, 63, i75-i76.
- [46] F. Demartin, C. M. Gramaccioli, I. Campostrini, Can. Mineral. 2008, 46, 447–453.
- [47] M. Lozinsek, T. Bunic, E. Goreshnik, A. Meden, M. Tramsek, G. Tavcar, B. Zemva, J. Solid State Chem. 2009, 182, 2897–2903.
- [48] K. Matsumoto, R. Hagiwara, Z. Mazej, E. Goreshnik, B. Žemva, J. Phys. Chem. B 2006, 110, 2138–2141.
- [49] T. Pilz, T. Schleid, M. Jansen, Z. Anorg. Allg. Chem. 2013, 639, 2555–2557.
- [50] G. Brunton, Acta Crystallogr. Sect. B 1968, 24, 1703–1704.
- [51] M. J. R. Clark, H. Lynton, Can. J. Chem. 1969, 47, 2579–2586.
- [52] I. Tiritiris, H. M. Bunz, T. Schleid, Z. Anorg. Allg. Chem. 2002, 628, 2212– 2212.
- [53] T. H. Jordan, B. Dickens, L. W. Schroeder, W. E. Brown, Acta Crystallogr. Sect. B 1975, 31, 669–672.
- [54] E. Goreshnik, A. Vakulka, B. Zemva, Acta Crystallogr. Sect. C 2010, 66, e9.
- [55] Q. W. Lin, W. D. Cheng, J. T. Chen, J. S. Huang, Chin. J. Struc. Chem. 1998, 17, 245–248
- [56] M. J. Dodge, Appl. Opt. 1984, 23, 1980-1985.
- [57] G. Tavcar, B. Zemva, Inorg. Chem. 2005, 44, 1525-1529.
- [58] J. Bonisch, G. Bergerhoff, Z. Anorg. Allg. Chem. 1981, 472, 35–41.
- [59] H. Fitz, B. G. Müller, Z. Anorg. Allg. Chem. 1997, 623, 579-582.
- [60] M. Y. Antipin, A. M. Ellern, V. F. Sukhoverkhov, Y. T. Struchkov, Y. A. Buslaev, J. Inorg. Chem. 1988, 33, 171–173.
- [61] J. Lin, M. H. Lee, Z. P. Liu, C. Chen, C. J. Pickard, Phys. Rev. B 1999, 60, 13380–13389.
- [62] C. T. Chen, G. Z. Liu, Annu. Rev. Mater. Sci. 1986, 16, 203-243.
- [63] S. J. Clark, M. D. Segall, C. J. Pickard, P. J. Hasnip, M. I. Probert, Z. Krist. Cryst. Mater. 2005, 220, 567–570.
- [64] B. G. Pfrommer, M. Cote, S. G. Louie, M. L. Cohen, J. Comput. Phys. 1997, 131, 233–240.
- [65] J. P. Perdew, K. Burke, M. Ernzerhof, Phys. Rev. Lett. 1996, 77, 3865–3868.
- [66] A. M. Rappe, K. M. Rabe, E. Kaxiras, J. D. Joannopoulos, *Phys. Rev. B* 1990, 41, 1227–1230.
- [67] J. S. Lin, A. Qteish, M. C. Payne, V. Heine, Phys. Rev. B 1993, 47, 4174– 4180
- [68] R. W. Godby, M. Schlüter, L. J. Sham, Phys. Rev. B 1988, 37, 10159–10175.
- [69] M. S. Hybertsen, S. G. Louie, *Phys. Rev. B* **1986**, *34*, 5390–5413.
- [70] C. T. Chen, Z. S. Lin, Z. Z. Wang, Appl. Phys. B 2005, 80, 1-25.
- [71] B. B. Zhang, M. H. Lee, Z. H. Yang, Q. Jing, S. L. Pan, M. Zhang, H. P. Wu, X. Su, C. S. Li, Appl. Phys. Lett. 2015, 106, 031906–031901.

Manuscript received: March 28, 2022 Revised manuscript received: May 4, 2022 Accepted manuscript online: May 7, 2022 Version of record online:

# **RESEARCH ARTICLE**

**Tetrafluoroborates** containing non- $\pi$ -conjugated [BF<sub>4</sub>] tetrahedra with alkali and/or alkaline-earth metals are suitable candidates for deep-ultraviolet optical materials, based on theoretical calculations. These compounds are comparable to the classical deep-ultraviolet material MgF<sub>2</sub>.



J. Sun\*, Z. Wu\*, Prof. M.-H. Lee, Prof. H. Duan\*

1 – 7

A Theoretical Perspective to Study the Optical Properties of Tetrafluoroborates

